Visualization of Combustion Within a Hybrid Rocket Motor

Elizabeth T. Jens: 05588428

EE 368: Final Project Report
Due Date: 5 June 2015

---

1 Introduction

A visualization facility has been developed at Stanford University in order to study flow in a turbulent combustion boundary layer. The motivation for the facility arises from recent studies of fast burning fuels for hybrid rocket propulsion where droplet lift-off from the melting fuel surface is the dominant mass transfer mechanism. The facility, shown in Figure 1, has been used to image the combustion of various fuels with gaseous oxygen. Five classical fuels have been tested, specifically Hydroxyl-Terminated PolyButadiene (HTPB) with 0.5% by mass carbon black, HTPB without carbon black, High Density PolyEtheylene (HDPE), Acrylonitrile Butadiene Styrene (ABS), and PolyMethyl MethAcrylate (PMMA) as well as a liquefying high regression rate fuel, specifically neat paraffin with 0.5% by mass of black dye, referred to as Blackened Paraffin (BP).

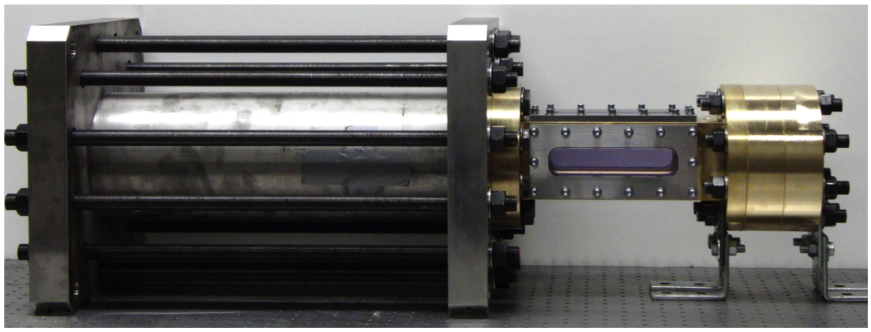

Figure 1: Stanford Combustion Visualization Facility. Oxidizer flow enters from the left and travels through the flow conditioning system before reaching the combustion chamber.

29 hot fires were successfully conducted in the combustion visualization facility in 2014. High speed color, schlieren and OH* chemiluminescence videos were recorded. Color videos are recorded with Casio Exilim EX-F1 cameras at 1200 frames per second with a resolution of 96 x 336 pixels. The schlieren imaging method adopted in this facility is the classical Z-type two mirror schlieren system. This configuration utilizes two identical mirrors with a focal length of 1.435 m set up in a Z-formation, as shown in Figure 2. A MotionPro X3 Plus camera and a 105 mm Nikon lens with an f-number of $f/2.8$ capture the schlieren images at 3000 frames per second with a resolution of 1080 $\times$ 236 pixels, 13 μsec exposure time, and a camera gain of 2.0. Images of OH* chemiluminescence are acquired at 3000 frames per second using a Photron APX i^2 intensified camera, a 105 mm Nikkor UV lens, and a high-transmission bandpass filter centered at 313 nm with a full-width half-max of 5 nm. All OH* images are acquired with an f-number of $f/8$ and a gain of 60% of the maximum gain of the camera. Gate times were adjusted to maximize signal while minimizing the risk of saturating the camera. At ambient pressure, the excited OH radical is primarily produced as a byproduct of reaction rather than thermal excitation [1], and when the excited OH molecules relax back to the ground state, they emit photons near 313 nm. The band-pass filter, which has an optical density of

4 outside of the pass band, blocks most of the black body emission from soot and chemilumenscence from other species (e.g. CH*) [2]. Therefore, by collecting the OH* emission, we obtain a global, path-integrated image of the reaction zone.

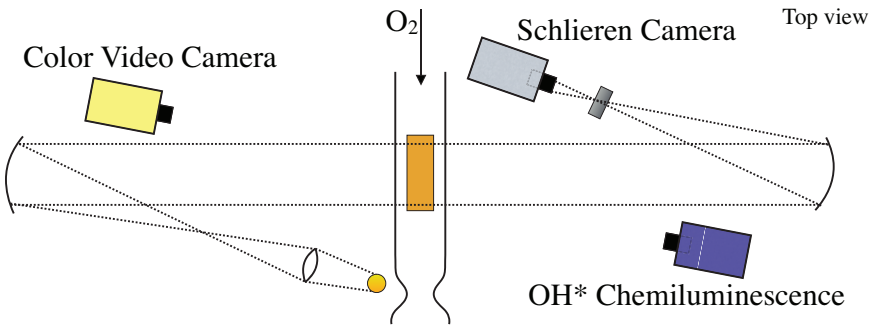

Figure 2: Schematic of test set-up with imaging equipment.

An example of each of the raw images is shown in Figure 3. At the outset of this project the author had access to data from 29 tests, this project focuses on the analysis of images from 11 of these tests (Test 13 - Test 23), and in particular on the analysis of the 14,207 schlieren images and 16,386 OH* chemiluminescence images collected for each of these tests. Note that the number of OH* chemiluminescence images exceeds the number of schlieren images due to the greater amount of on-board storage on the Photron APX i^2 camera as compared to the MotionPro X3 Plus. This work was divided into a number of tasks and subtasks, all aimed towards applying the techniques covered in EE278 in order to better understand the combustion process with hybrid rocket motors. The specific tasks and the approach taken toward achieving them are discussed in the methodology.

2 Methodology

2.1 Correcting OH* Images

The UV sensitive Photron APX i^2 camera used to collect the OH* images was slightly damaged, resulting in bad pixel values in certain columns within each image. An example of the raw images produced by the camera is show in Figure 4. The damaged pixels occupied specific columns within each image but the number and location of the columns that were affected varied from test to test. The values of the damaged pixels did not remain constant, they could occupy any value from 0 to 1. Extensive analysis of the raw images revealed that although the columns containing the damaged pixels varied, they were always a subset of the same group of columns. Any columns that contained any values exactly equal to 0 or 1 typically represented damaged columns, as with normal operation the camera was not saturating or underexposed. All columns that contained these values were identified for each test. These potentially damaged columns were then compared across all tests, and any columns that appeared to be damaged in multiple tests were flagged. Code was then developed to step through each of these columns and find any pixels greater than 2 standard deviations from the median of itself and the 2 pixels to either side. These pixels were replaced with the mean value of the pixel to either side of it. This approach was adopted to minimize the affect of any standard filtering operation on the undamaged majority of the OH* pixels. An example of the results of this process is shown in Figure 4.

2.2 Aligning OH* and Schlieren Images

The schlieren and OH* images needed to be aligned in order to gain insight into where combustion takes place within the turbulent boundary layer above hybrid rocket fuels. The process for doing this was divided into two steps, first projecting the images onto the same plane with the same scale, then lining the images up by focusing on the alignment of the leading edge of the fuel grain.

(a) Raw Color Image

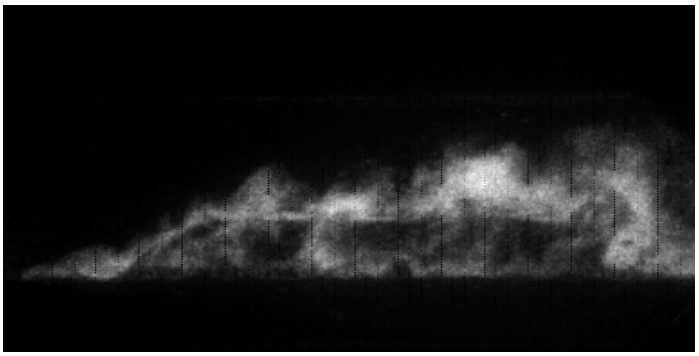

(b) Raw OH* Image

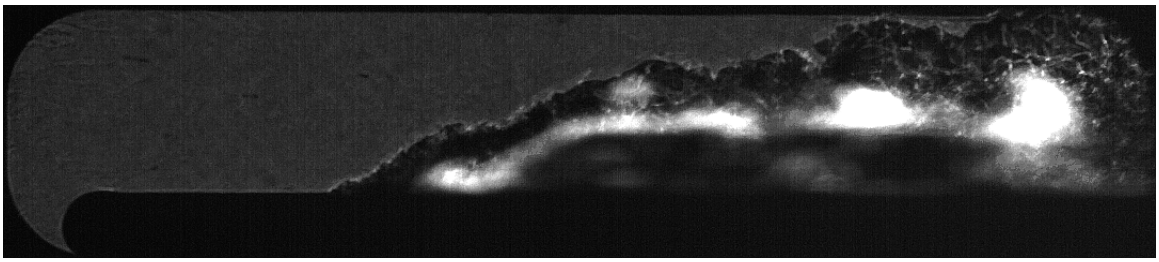

(c) Raw Schlieren Image

Figure 3: Examples of raw image from each camera. Test shown is the combustion of BP with gaseous oxygen at elevated pressure.

2.2.1 Projecting Images

The schlieren and OH* images were triggered together and recorded at the same frame rate. However, it was not possible to give both cameras a square view of the test section simultaneously. Some projection error in the OH* images was inevitable since schlieren optics require a straight uninterrupted path through the test section. Figure 2 shows the test set-up and the location of the cameras. It can be seen that the OH* camera does not sit perpendicular to the test section, but rather sits an angle of approximately 15 degrees[1]. Future work could consider the use of a beam-splitter to negate the need for this correction and to remove any bias in the OH* images resulting from integrating the signal through an off-normal path; however, an appropriate beam-splitter was not available at the time of this work.

A method was developed to remove projection error and to ensure consistent alignment of OH* and schlieren images regardless of their scale. Grid images were taken prior to each test. The raw OH* images were affected by some noise, the signal to noise ratio in the OH* grids was improved by taking the mean of many OH* grid images prior to analyzing them. The separation of the gridpoints in "real-space" is known apriori to be dx = 5.08 mm (0.2 in) and dy = 2.54 mm (0.1 in). The gridpoints are detected using a scheme originally developed by Miller [3] that was modified

[1]This projection angle is calculated by looking at the mean horizontal distortion of the OH* grid images

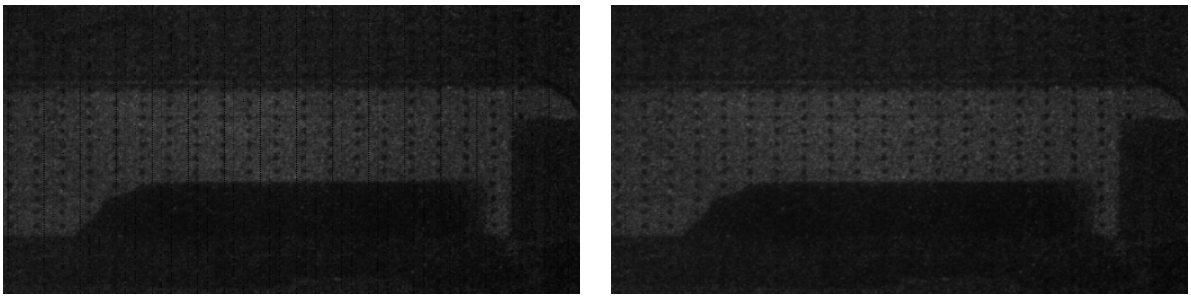

(a) Raw OH* Image (b) OH* Image with Damaged Pixel Removal

Figure 4: Test 22. Grid image with and without damaged pixel removal.

for this purpose. The user must first manually identify the three gridpoints in the bottom left of the image. The algorithm then evaluates the pixel intensities around each of these points and fits a Gaussian to these intensities; the center of the gridpoint is taken as the center of the fitted gaussian. The extent of the region to be evaluated around the gridpoint is defined to be a window of ± 3 pixels. The code then estimates the expected number of pixels between gridpoints (both in the horizontal and vertical directions), estimates a new center for the next gridpoint, re-evaluates the Gaussian in the region around this point and finds the new center location. This process is repeated across each row and up all columns to be evaluated. Figure 5 shows an example of detected gridpoints overlaid over the schlieren grid image. In this way the code adjusts for any error introduced by the user in selecting the original gridpoints or any distortion to the grid introduced by the optics. After identification, a 2D cubic polynomial is fit to the location of all of the gridpoints to map the x,y location in pixel space to the x,y location in real space. The location of the schlieren and OH* pixels in real space is then known. However, this process has not yet projected the images onto the same plane, it has simply determined the mapping of the images to their location in real space. The schlieren and OH* images now need to be projected onto the same uniform grid in order to overlay them. A uniform grid of x,y locations in real space is generated such that there is no reduction in resolution for either image. For all images, a uniform grid was generated such that a single pixel represents 0.1 mm in each direction. This typically scaled the images to a little over 1.5 times their initial size. With this methodology, the schlieren and OH* images were transformed to have the same size and scale, but in order to concurrently analyze and display them they needed to be aligned, the approach for this is described in the following subsection.

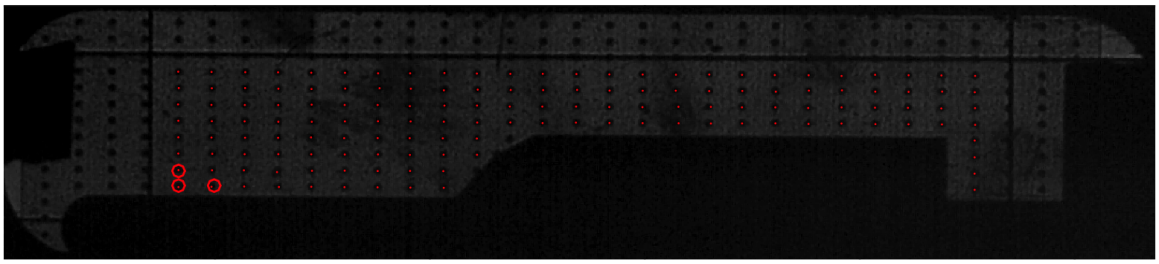

Figure 5: Example of detected grid points for schlieren grid image.

2.2.2 Overlaying Images

The images were not able to be aligned directly by overlaying a single grid point due to the difference in the location of the gridpoints relative to the test article. This difference is an artifact of projection error applied to the normal distance between the physical grid and test article. The grid image was installed in front of the test section, and the fuel grain sits within the test section, thus, the location

of the gridpoints relative to the fuel grain as seen by the OH* camera was different to the location of those same points in the schlieren images. As an example, the point immediately ahead of the fuel grain in the schlieren image would typically sit within the fuel grain in the OH* image. An alternative alignment approach was required. Initially, cross correlation of the two images was the intended alignment method, however, the slight distortion of the fuel grain leading edge profile in the OH* images resulting from re-projection of the image led to a very low signal to noise ratio in the phase correlation. Thus, a clear cross correlation peak corresponding to the alignment of the two images was not always able to be identified. Instead, simple minimization of squared difference per pixel between the images was used in order to align them. The fore end of the fuel grain is the region around which accuracy is required, and thus only the region around the front of the fuel grain was used to align the OH* images to the full schlieren images. Care had to be taken to only look at the overlapping region of the two images. This approach worked successfully for aligning the images in all 11 tests.

Following alignment, it was desirable to display the aligned schlieren and OH* images using a custom colormap to false-color the OH* images. Matlab does not allow the use of two distinct colormaps to be used in a single figure. Thus, in order to display greyscale schlieren images overlaid with false-color OH* images, the schlieren images were converted to RGB with equal weights in all three components, producing the desired greyscale image. The OH* images were overlaid over the schlieren image with the custom violet colormap and a transparency of 50%. An example of the figures produced with these display properties is shown in Figure 6.

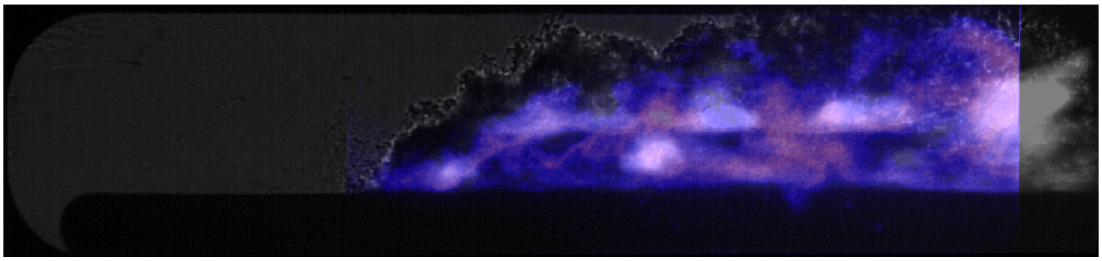

Figure 6: Example overlaid schlieren and OH* image. The image shown is for the combustion of BP and oxygen at elevated pressure.

2.3 OH* Intensity

The mean intensity within the OH* chemiluminescence images was investigated in order to quantify the burn time, and compare that with the burn time determined from the pressure trace. The variations in mean intensity with time also give insight into the unstable nature of the flames. The approach for this work was very straightforward, the mean pixel value for each image was calculated across the entire re-projected image. The values of mean intensity were then normalized to range from 0 to 1. Future work for this task will focus on overlaying the results of this analysis with the combustion chamber pressure versus time trace in order to investigate the correlation between the number of OH* radicals and the chamber pressure.

2.4 Edge Detection

One of the major contributions from the combustion visualization tests is the quantification of the growth rate of the turbulent boundary layer, and the flame location within that boundary layer, for typical hybrid motor operating conditions.

2.4.1 Fuel Grain

The fuel grain location was initially estimated from the profile of the fuel grain prior to ignition. The first schlieren image for each test was used for this purpose. The image was gaussian filtered

then binarized using Otsu's method. Following binarization, small dark regions and white holes were removed. The Canny edge detector was then applied to trace the fuel grain profile. The Canny edge detector first smooths the image with a Gaussian filter, in this case a standard deviation of $\sigma = 1.1$ was used for the filtering operation. The Canny edge detector approximates gradient magnitude and angle across the image, applies non-maxima suppression to the gradient magnitude, then uses double thresholding to detect strong and weak edge pixels. All weak edge pixels not connected with strong edge pixels are rejected. Thresholds of 0.2 and 0.5 were found to be successful threshold values for the weak and strong edges, respectively. Following the application of the edge detector the region surrounding the fuel grain was then isolated to remove undesired window edges around the periphery of the image. This approach with these inputs successfully identified the fuel grain edge in the first schlieren image for all tests. An example of the resulting fuel grain trace is shown in Figure 7.

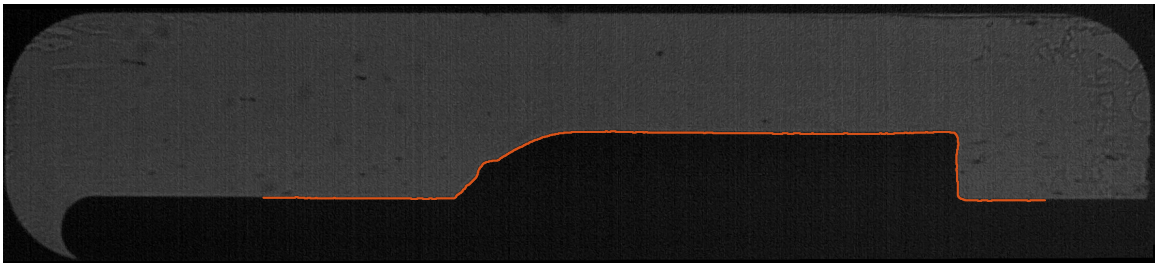

Figure 7: Fuel grain edge detection overlaid on grayscale schlieren image. The image shown is for the combustion of BP and oxygen at elevated pressure.

2.4.2 Flame Location

The flame location was quantified by looking at the mean OH* chemiluminescence images. Hybrid rocket combustion theory assumes an infinitely thin flame sheet. Thus, the first step in quantifying the flame location involved approximating the combustion zone as a region of unit pixel thickness. The location of the flame was assumed to be the location of peak OH* intensity within each column in the vicinity of the the fuel grain. In order to avoid the inclusion of noisy points far from the main flame front, each column was only included if the peak intensity exceeded a threshold of 0.05. Future work should look at evaluating the thickness of the flame sheet by investigating the vertical distribution of the flame at various points along the fuel grain.

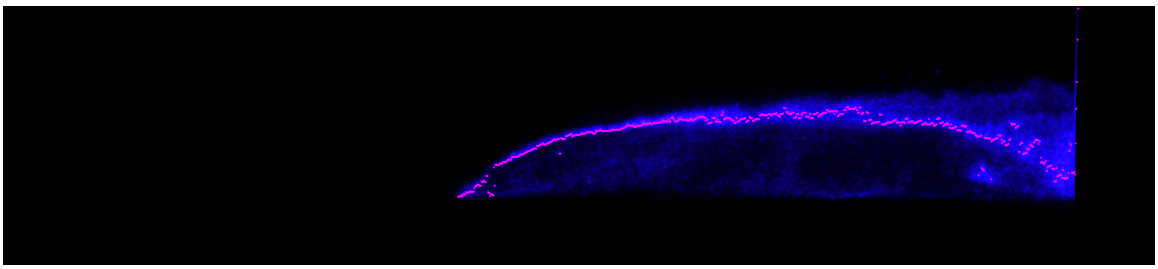

Figure 8: Flame location identification overlaid on OH* image with custom colormap. The image shown is for the combustion of BP and oxygen at elevated pressure.

2.4.3 Boundary Layer

Detecting the boundary layer in the mean images proved somewhat challenging. In general the variations in image intensity within the freestream are less than those within the boundary layer and the boundary between these two regions can easily be identified with the naked eye. However,

all attempts to use this knowledge to directly differentiate and/or threshold the image proved unsuccessful. The direct application of standard edge detectors and filters covered in EE368 could not be applied as these methods always picked up on features and gradients in the freestream and within the boundary layer. This is an issue that has been encountered by others working with schlieren images, see references [4, 5, 6]. The approach that proved successful for this work involved the adoption of the 2D bilateral filter adopted by Smith [7, 4, 5] as well as the use of the matlab entropy filter [8].

The 2D bilaterial filter is an edge preserving filter that minimizes the difference in like regions whilst preserving strong edges [7]. The bilateral filter applies a Gaussian kernal on the domain and range of the image, for this work standard deviations of $\sigma_d = 4$ and $\sigma_r = 0.1$ were used for the domain and range respectively. The width of the kernal was defined to be $w = 3\sigma_d + 1$. The affect of the bilateral filter on the mean schlieren image and the entropy filtered image is shown in Figure 9. The matlab entropy filter was applied after bilateral filtering using a disk structuring element with a radius of 3 pixels. The entropy filter converts each pixel location to a value representing the statistical measure of randomness in the region around that pixel. The entropy filter is sensitive to noise and thus the application of the bilateral filter prior to applying the entropy filter was required. This can be most clearly seen by looking at the result of entropy filtering with and without bilateral filtering, Figure 9. The output values from the entropy filter were scaled to the default range for a greyscale image and the image was binarized using Otsu's method. Small and medium regions less than 1000 pixels in size were then removed. The high intensity region of the image, corresponding to the boundary layer, was eroded using a disk structuring element of radius 10 in order to counter the dilative effect of the entropy filter. The Canny edge detector was then applied using $\sigma = 1.1$ again for the Gaussian filter along with weak and strong edge thresholds of 0.1 and 0.5, respectively. The region around the fuel grain was isolated and small positive regions less than 500 pixels in size were again removed. The second application of small region removal was required to remove any edges that were previously connected to the window frame. This approach isolated edges around the the boundary layer and the base of the fuel grain. The x,y locations of this edge were found and the upper region, corresponding to the boundary layer edge, was isolated.

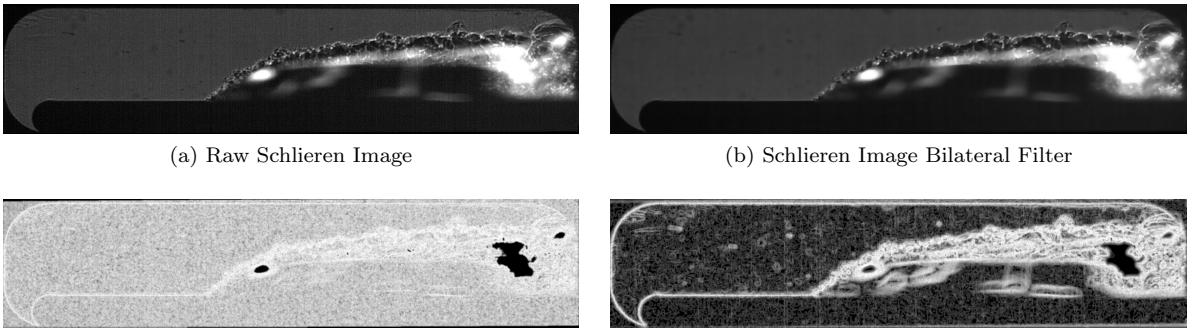

(a) Raw Schlieren Image

(b) Schlieren Image Bilateral Filter

(c) Schlieren Image Entropy Filter

(d) Schlieren Image Bilateral then Entropy Filter

Figure 9: Test 26. Effect of bilateral and entropy filters on schlieren image. The image shown is for the combustion of BP and oxygen at elevated pressure.

3 Results

The projection and alignment code was successfully implemented on all images (11 tests with 14,207 schlieren images and 16,386 OH* chemiluminescence images).

The edge detection algorithm described above was applied to numerous test images. The algorithm appeared to perform well on individual images of both atmospheric chamber pressure and

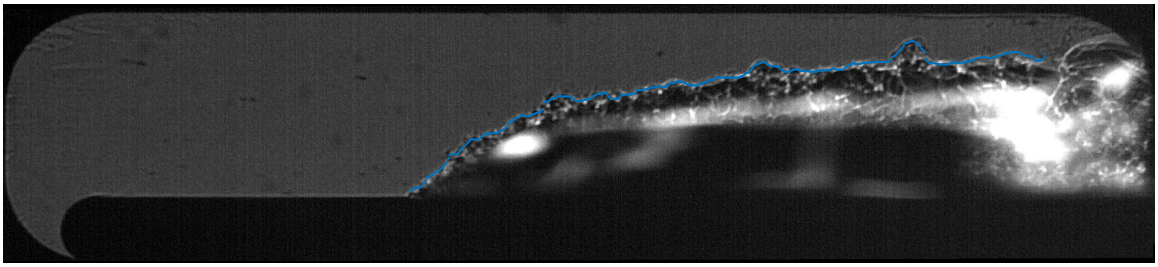

Figure 10: Test 26. Boundary layer edge detected overlaid on schlieren image. The image shown is for the combustion of BP and oxygen at elevated pressure.

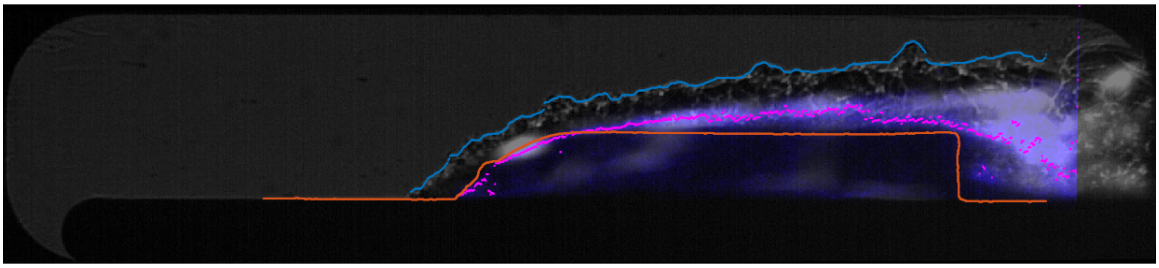

Figure 11: Test 26. Boundary layer edge, flame location and original fuel grain shape overlaid on grayscale schlieren and OH* image with 50% transparency and custom colormap. The image shown is for the combustion of BP and oxygen at elevated pressure.

elevated chamber pressure tests. In order to reduce computation time, the mean profiles of many consecutive images were analyzed. For atmospheric tests the edge detection analysis was conducted on mean images of 50 consecutive images. Some example results are shown in Figure 12.

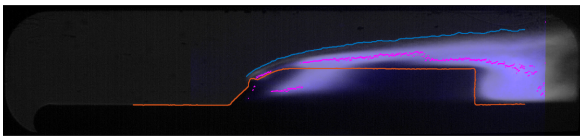

(a) Test 18. Clear HTPB

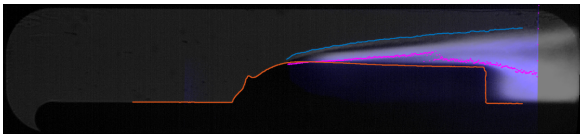

(b) Test 25. HTPB

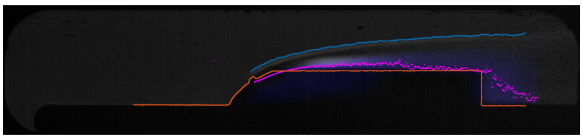

(c) Test 19. HDPE

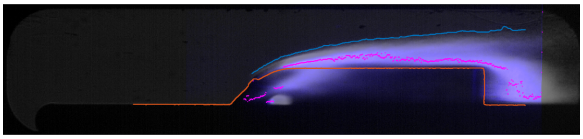

(d) Test 20. ABS

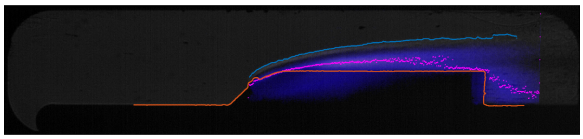

(e) Test 22. BP

Figure 12: Example edge detection results for 50 consecutive mean images during atmospheric pressure tests.

There is significant oscillation in the boundary layer thickness and OH* intensity within the pressurized test images. The methodology described in this report did not successfully detect the boundary layer edge for the pressurized test mean images, see Figure 13.

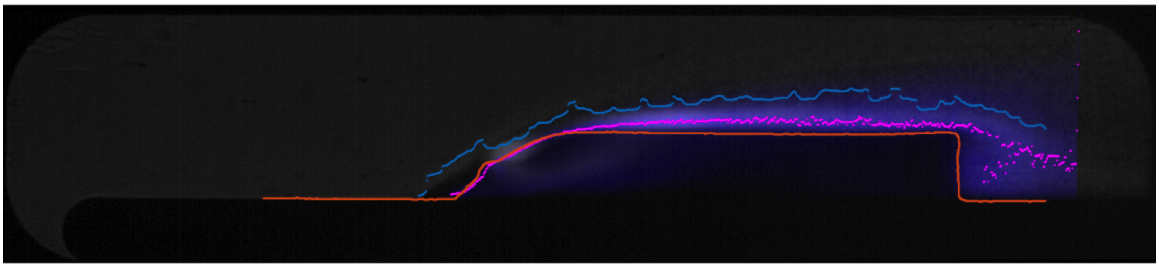

Figure 13: Test 26. Example failed attempt at edge detection for 50 consecutive mean images during elevated pressure test.

4 Future Work

The next major challenge in the work is approximating the instantaneous fuel grain location during a test. This cannot be directly inferred from the images and so will need to be estimated using hybrid combustion theory. Once the code for this is in place, the image processing code and the fuel location calculations will need to be run across thousands of images for each test.

References

[1] Hall, J. M. and Petersen, E. L., "An optimized kinetics model for OH chemiluminescence at high temperatures and atmospheric pressures," *International Journal of Chemical Kinetics*, Vol. 38, No. 12, 2006, pp. 714–724.

[2] Kojima, J., Ikeda, Y., and Nakajima, T., "Spatially resolved measurement of OH*, CH*, and C2* chemiluminescence in the reaction zone of laminar methane/air premixed flames," *Symposium (International) on Combustion*, Vol. 28, No. 2, 2000, pp. 1757–1764.

[3] Miller, V. A., *High-speed Tracer-based PLIF Imaging for Scramjet Ground Testing*, Ph.D. thesis, Stanford University, 2014.

[4] Smith, N. T., Lewis, M. J., and Chellappa, R., "Extraction of Oblique Structures in Noisy Schlieren Sequences Using Computer Vision Techniques," *AIAA journal*, Vol. 50, No. 5, 2012, pp. 1145–1155.

[5] Smith, N. T., *Schlieren sequence analysis using computer vision*, Ph.D. thesis, University of Maryland, 2013.

[6] Smith, N. T., Lewis, M. J., and Chellappa, R., "Detection, Localization, and Tracking of Shock Contour Salient Points in Schlieren Sequences," *AIAA journal*, Vol. 52, No. 6, 2014, pp. 1249–1264.

[7] Tomasi, C. and Manduchi, R., "Bilateral filtering for gray and color images," *Computer Vision, 1998. Sixth International Conference on*, IEEE, 1998, pp. 839–846.

[8] Gonzalez, R. C., Woods, R. E., and Eddins, S. L., *Digital image processing using MATLAB*, Pearson Education India, 2004.